

# Towards an experimental control of neural activity: The Wilson-Cowan model <sup>\*</sup>

Sebastián Martínez <sup>\*,\*\*</sup> Ricardo S. Sánchez-Peña <sup>\*,\*\*\*</sup>  
Mariano Belluscio <sup>\*\*\*\*</sup> Joaquín Piriz <sup>†</sup>  
Demián García-Violini <sup>\*\*,\*\*\*</sup>

<sup>\*</sup> *Depto. de Investigación y Doctorado, Instituto Tecnológico de Buenos Aires (ITBA), Argentina. (e-mail: semartinez[rsanchez]@itba.edu.ar).*

<sup>\*\*</sup> *Depto. de Ciencia y Tecnología, Universidad Nacional de Quilmes, Bernal, Argentina (e-mail: ddgv83@gmail.com)*

<sup>\*\*\*</sup> *CONICET, Argentina*

<sup>\*\*\*\*</sup> *IFIBIO, Facultad de Medicina, UBA-CONICET*

<sup>†</sup> *IFYBINE, Ciudad Universitaria, UBA-CONICET*

---

**Abstract:** The prospect of modifying neural activity in a principled way, could facilitate the understanding of brain functions and the development of medical treatments. To predict the dynamics that underlie the different brain activities, several neurobiological models have been proposed, either focusing on individual cells or whole populations. In this context, control systems are a powerful tool to provide a correct articulation between inputs, i.e. neural stimuli, and observables, i.e. system outcomes. Based on well-established neurobiological hypotheses, this study presents a control framework to regulate a neural-mass activity, with potential uses for pattern tracking, such as, rhythm evoking and phase synchronisation. Being these mechanisms closely connected with real brain computations, this study is carried out using a meaningful perspective in terms of biological interpretation. To this end, the Wilson-Cowan model is used, where the input stimuli is elicited through light signals applied to genetically modified neurons that express light-gated actuators. Thus, this study states a crucial proof of concept towards a future experimental application of the control framework for neurobiological systems.

*Keywords:* Wilson-Cowan; closed loop; control systems; neural model; optogenetics.

---

## 1. INTRODUCTION

Closed-loop neuroscience is showing a rapid development. In addition to technical advances, this is mainly driven by its huge potential for causal investigation of ongoing neural processes and circuits, as well as, the promise to constitute effective treatments for disorders and diseases. In recent years, this boom has gone *'hand-in-hand'* with advances in brain imaging (Kim et al., 2018), to probe and measure neural activity (sensing) and intervention (Deubner et al., 2019), to physiologically modify the variables of interest (actuation). A large portion of the existing body of work has been carried out empirically, from well-documented observations, in pursuit of neural modulation. By way of example, the standard deep brain stimulation (DBS) protocol is based on trial and error procedures (Mirza et al., 2019). Control system theory can establish a framework, from both the analysis and design perspectives, for closed-loop modulation schemes. This approach can provide powerful tools, with proven effectiveness, that have been the standard in complex areas such as industrial processes, satellite navigation, energy generation, and medicine, to name a few.

Considering complex neurobiological structures as dynamical systems with defined inputs and outputs, allows for tackling different modulation/tracking problems using control strategies. Most of these approaches are within the scope of model-based control, i.e. the dynamic evolution of the system is predicted online with a suitable model in order to compute an appropriate control signal with a controller.

The available models range from biologically detailed descriptions, in terms of interactions and connectivity, to biologically realistic bulk simplifications. The selection of these models relies on, for example, the circuit under study and the required detail level, computational cost, and/or need for online running. Remarkably, for neuron population modeling, there are simplified models that are particularly fast to simulate while describing relevant observed phenomena, and thus suitable for a control framework. These are often referred to as neural-mass models (Coombes and Byrne, 2019). Using ensembles of neurons that belong to a certain cluster, defined, for example, by type or function, the dynamical behavior of the whole set under study is described with properties such as mean firing rate or voltage. This characterization, wherein many individual neurons is treated as average interaction, comprises a mean-field technique, as the case of the Local Field Potential (LFP).

---

<sup>\*</sup> This research has been financially supported by grant PICT2017-2417 from the ANPCyT, Argentina.

Our goal, specifically, is to transiently replicate a particular brain rhythm, in a phased-locked way, using a closed-loop control strategy. Nevertheless, this approach can be modified based on several observed phenomena. Other types of synchronizations can be established, for example between different oscillators (Faedo et al., 2021), and also, based on other functional interactions e.g. frequency-amplitude (Srinivasan et al., 2013).

The remainder of this paper is organised as follows. In Section 2, the chosen dynamical model is introduced, and the principal biological assumptions are highlighted. Section 3 elaborates on the system structure, and explains the proposed control strategy. In Section 4, a specific case study, based on experimental observations and a particular control methodology, is stated and solved in simulation. Finally, Section 5 discusses the conclusions from this study, towards an experimental implementation.

## 2. BIOLOGICAL HYPOTHESIS AND MODELING

In most neural mass models, the system is described using nonlinear differential equations to capture the dynamics of its states, usually, defined in terms of physical interactions. Common variables of choice include (neural) population activities or rates. They characterize the proportion of cells activated per unit time, i.e. the spiking neurons, in a bounded volume of tissue. The synaptic inputs of the single neurons that belong to the arrangement are modeled with the system inputs. In addition, a nonlinear mapping models the input-output characteristic of each neural population, similarly to a frequency-current curve (gain function) of single neurons (Powers and Binder, 2001). Wilson and Cowan proposed a mean-field theory for neural activity (Wilson and Cowan, 1972), deriving coupled nonlinear differential equations for spatially localized excitatory and inhibitory sub-populations. The assumption that local cells share similar properties and responses is supported by the redundancy of processes, and the dense interconnection between them. Under these assumptions, the space-clamped Wilson-Cowan model (W-C), i.e. without considering spatial gradients, can be expressed as:

$$\begin{aligned}\tau_E \dot{E} &= -E + (1 - rp_E E) f_E \{ w_{EE} E - w_{EI} I + P \}, \\ \tau_I \dot{I} &= -I + (1 - rp_I I) f_I \{ w_{IE} E - w_{II} I + Q \}.\end{aligned}\quad (1)$$

Each subpopulation activity presents an exponential decay with time constant  $\tau_i$ ,  $i \in \{E, I\}$ , associated with the propagation of postsynaptic potentials. The nonlinear-weighting input term gives the proportion of cells for each subpopulation that would respond to the level of excitation between curly braces. That expressions highlight the functional coupling (in a feedback way, i.e. each subpopulation with itself, and in a feedforward way, i.e. between subpopulations), as weighted by the positive constants  $w_{ij}$ ,  $i, j \in \{E, I\}$ , representing the average number of synapses per cell. In the most general case, each subpopulation receives at least inputs from the other, driving the rate of change of each activity,  $\dot{E}$  and  $\dot{I}$ . The response function  $f_i \{ \cdot \}$ ,  $i \in \{E, I\}$ , is typically sigmoidal, i.e. the activation of cells monotonically increases with sufficient stimulus level. The factors  $(1 - rp_i)$ ,  $i \in \{E, I\}$ , denote the proportion of cells that could fire, since it is used to account for the spiking refractory period, and  $P$  and

$Q$  are external current-like inputs. These inputs can be adapted for optogenetic actuation, considering inhibitory and excitatory opsins<sup>1</sup>. The light-to-current mappings

$$\begin{cases} \mathcal{O}_E : L_E \longrightarrow P, \\ \mathcal{O}_I : L_I \longrightarrow Q, \end{cases}\quad (2)$$

could be algebraic expressions linking, for example, applied light intensities ( $L_E$  and  $L_I$ ) with transmembrane net currents ( $P$  and  $Q$ ), or even differential equations that describe the opsins own dynamics (Williams et al., 2013). In this control framework, those dynamics could be added to the system model. However, and without loss of generality, in a general case where the mappings in Eq. (2) are much faster than the system time-constants, these relationships can be neglected. A complete model, including the dynamical descriptions in Eq. (2), will be the subject of an extension of this study.

The W-C model exhibits strongly-nonlinear system properties. These include multistability, hysteresis, and limit cycle behavior, that depend, particularly, on the parameters choice and inputs. In Fig. 1, a typical open-loop response of the W-C system is depicted in the  $I$ - $E$  phase space, for varying levels of the excitatory input  $P$ . Remarkably, the system undergoes a qualitative change of behavior, from a) damped oscillations to c) sustained oscillations.

## 3. CONTROLLER AND ESTIMATOR ANALYSIS

From equation (1), the W-C model can be reformulated as follows:

$$\begin{bmatrix} \dot{E}(t) \\ \dot{I}(t) \end{bmatrix} = \begin{bmatrix} \frac{1}{\tau_E} & 0 \\ 0 & \frac{1}{\tau_I} \end{bmatrix} \left\{ - \begin{bmatrix} E(t) \\ I(t) \end{bmatrix} + \underbrace{\begin{bmatrix} f_E(\gamma_{xE} + P) \\ f_I(\gamma_{xI} + Q) \end{bmatrix}}_{u_{\text{kti}}(t)} \right\}, \quad (3)$$

$$u_{\text{kti}}(t) = \begin{bmatrix} \tilde{u}_1(t) \\ \tilde{u}_2(t) \end{bmatrix} = \begin{bmatrix} f_E(\gamma_{xE} + P) \\ f_I(\gamma_{xI} + Q) \end{bmatrix} \triangleq \begin{bmatrix} f_E(u_p) \\ f_I(u_q) \end{bmatrix}, \quad (4)$$

where the sigmoid activation function is

$$\begin{aligned}f_i(x) &= \frac{1}{1 + e^{-a_i(x - \theta_i)}} - k_i \in [-k_i, 1 - k_i], \\ k_i &= \frac{1}{1 + e^{-a_i \theta_i}} \quad \text{constant.}\end{aligned}$$

The corresponding inverse sigmoid function is

$$x = -\frac{1}{a_i} \ln \left( \frac{1}{f_i + k_i} - 1 \right) + \theta_i \in \mathbb{R},$$

with  $i \in \{E, I\}$  for each case, with gain  $a_i$  and threshold  $\theta_i$  as indicated in Fig. 2. For the sake of simplification, the refractory period terms in equation (1) have been dropped, i.e.  $rp_E = rp_I = 0$ , since they do not affect substantially the system dynamics (Wilson and Cowan, 2021).

The state is composed of the excitatory  $E(t)$  and inhibitory  $I(t)$  activities. In this case, the output of the system  $y(t)$  is the LFP, which can be modelled as a summation of both activities ( $E(t)$  and  $I(t)$ ), i.e. a linear

<sup>1</sup> The opsins are light-activated ion channels (Deisseroth, 2011), that could be artificially expressed in the neuron membrane.

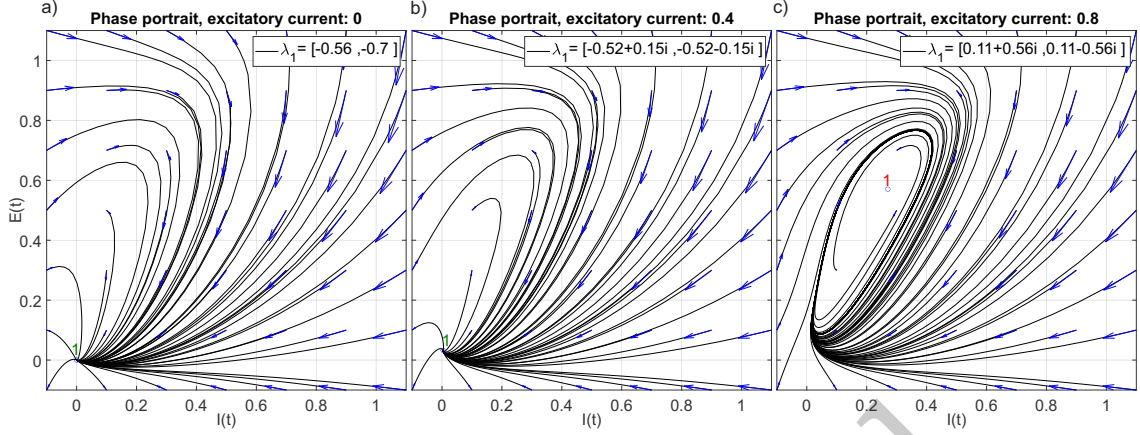


Fig. 1. Open loop response of the W-C system for varying levels of excitatory current stimulus  $P$ , and the eigenvalues of its corresponding jacobian linearization matrices. a) For  $P = 0$ , the W-C system shows an isolated equilibrium point (stable node) at the origin of the phase space. b) The input  $P = 0.4$  shifts the equilibrium point, and changes its nature to a stable focus. c) For inputs  $P = 0.8$  and above, the equilibrium point becomes an unstable focus, and the system shows oscillatory dynamics, as depicted with the closed, isolated, stable attractor (limit cycle).

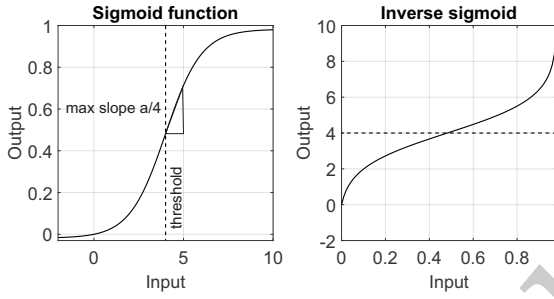


Fig. 2. The activation sigmoid function and its inverse. The threshold  $\theta_i$  is defined as the input with the maximum slope of the curve,  $a_i/4$ , with  $i \in \{E, I\}$ .

combination through constants  $c_1$  and  $c_2$  that balance each contribution:

$$y(t) = [c_1 \ c_2] \begin{bmatrix} \hat{E}(t) \\ \hat{I}(t) \end{bmatrix}. \quad (5)$$

The  $\gamma_{xi}(t)$  functions, introduced for Eqs. (3) and (4), are defined as:

$$\begin{aligned} \gamma_{xE}(t) &= w_{EE}\hat{E}(t) - w_{EI}\hat{I}(t), \\ \gamma_{xI}(t) &= w_{IE}\hat{E}(t) - w_{II}\hat{I}(t). \end{aligned} \quad (6)$$

Here  $[\hat{E}(t), \hat{I}(t)]^T$  are the estimations of the state, computed by means of an Extended Kalman filter (EFK) (Ribeiro, 2004), as indicated in Fig. 3. Hence, the manipulated-input signals are obtained as:

$$\begin{bmatrix} P \\ Q \end{bmatrix} = \begin{bmatrix} u_p - \gamma_{xE} \\ u_q - \gamma_{xI} \end{bmatrix} = \begin{bmatrix} -\frac{1}{a_E} \ln\left(\frac{1}{u_1+k_E} - 1\right) + \theta_E - \gamma_{xE} \\ -\frac{1}{a_I} \ln\left(\frac{1}{u_2+k_I} - 1\right) + \theta_I - \gamma_{xI} \end{bmatrix}, \quad (7)$$

where  $[u_1(t), u_2(t)]$  are the components of  $u_{sat}$  as depicted in Fig. 3.

A stabilizing controller  $K_{LTI}$  can be computed with input  $e(t)$  and output  $u_{lti}$  as indicated in Fig. 3 for the Linear time-invariant (LTI) model (3)-(5), that can be represented with a transfer matrix  $G(s)$  in the Laplace domain. It is of particular interest, a controller design focused on a tracking problem, e.g. the tracking of oscillatory references

to evoke rhythms of biological significance. Uncertainty plays a crucial role in complex biological systems, therefore, robustness and performance should be considered in order to account for that dynamic uncertainty (Zhou et al., 1996; Sánchez Peña and Sznaiier, 1998). This will be explained in subsection 3.1.

The controller output is vector  $u_{lti}$  in (4) from which the input signals can be obtained through state estimation and equation (7). Nevertheless, due to the fact that the pairs  $\tilde{u}, u_p$  and  $\tilde{u}_2, u_q$  are related through the inverse sigmoid function, the values of  $\tilde{u}_j$ , should be bounded in the interval  $[-k_i, 1-k_i]$ . Therefore, the saturated control signal  $u_{sat}$  can be defined as:

$$u_{sat}(t) = \begin{cases} 1 - k_i & \text{if } \tilde{u}_j \geq 1 - k_i, \quad (j = 1, 2) \\ -k_i & \text{if } \tilde{u}_j \leq -k_i, \quad (j = 1, 2) \\ u_{lti}(t) & \text{otherwise} \end{cases}$$

Fig. 4 represents the saturation of each LTI signal in the interval  $[-k_i, 1-k_i]$  which leads to the saturated control signal  $u_{sat}$ . From its the definition, the gain of this nonlinear operator, as depicted in Fig. 3, is less than one. Therefore the small gain theorem can be used to prove closed-loop stability of the nonlinear system (Sánchez Peña and Sznaiier, 1998).

### 3.1 Stability analysis

The previous LTI model  $G(s) : u_{lti} \rightarrow y$ , is a diagonal multiple-input multiple-output (MIMO) system. Next, the closed-loop system represented in Fig. 3 can be transformed into a combination of an LTI model and an "uncertainty"<sup>2</sup> block  $\Delta = \text{diag}\{\Delta_E, \Delta_I\}$ , which is defined as follows,

$$\Delta_i \triangleq \begin{cases} u_{\delta_j} = \tilde{u}_j > 1 - k_i & \rightarrow y_{\delta_j} = 1 - k_i, \quad (j = 1, 2) \\ u_{\delta_j} = \tilde{u}_j \in [-k_i, 1 - k_i] & \rightarrow y_{\delta_j} = \tilde{u}_j, \quad (j = 1, 2) \\ u_{\delta_j} = \tilde{u}_j < -k_i & \rightarrow y_{\delta_j} = -k_i, \quad (j = 1, 2). \end{cases}$$

The latter represents the difference between signals  $u_{lti}$  and  $u_{sat}$ , as indicated in Fig. 4 with a dashed line. Hence

<sup>2</sup> Actually this is not real uncertainty, it is a convenient interpretation that replaces a nonlinearity with an LTI model plus a bounded  $\Delta$  block.

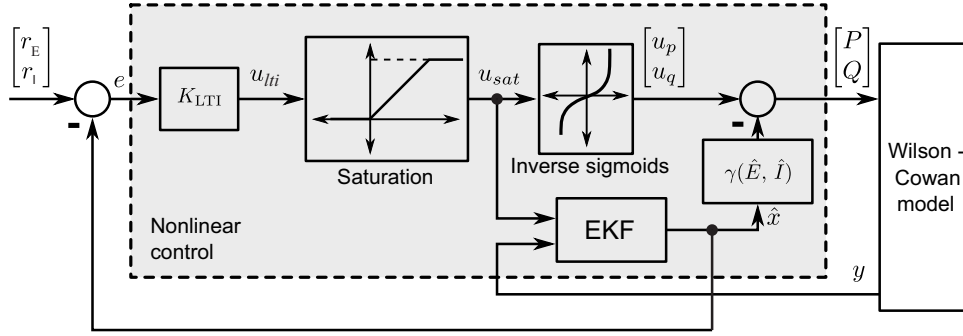


Fig. 3. Nonlinear control connected with the Wilson-Cowan equations.

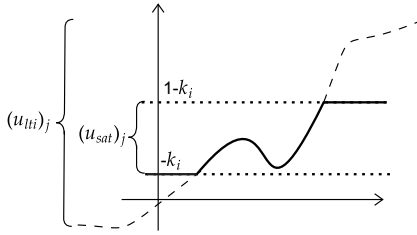


Fig. 4. Linear time-invariant ( $u_{lti} = [\tilde{u}_1 \tilde{u}_2]^T$ ) vs. saturated control ( $u_{sat} = [u_1 u_2]^T$ ).

the gain of the  $\Delta : u_\delta \rightarrow y_\delta$  operator according to its definition is  $\|\Delta\| \leq 1$ . Thus, considering the complementary sensitivity function (LTI closed-loop transfer matrix),

$$T(s) = K_{LTI}(s)G(s) [I + K_{LTI}(s)G(s)]^{-1}, \quad (8)$$

schematically depicted in Fig. 5, the internal stability of this connection can be theoretically defined, as discussed in the following.

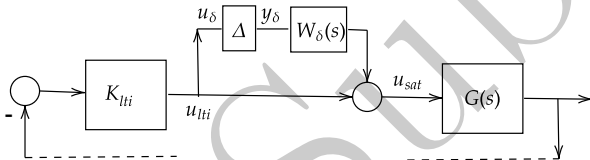


Fig. 5. LFT structure considered for the nonlinear closed-loop stability analysis.

The same framework could be used to add actual dynamic uncertainty represented by a filter  $W_\delta(s)$  in series with  $\Delta$  as in Fig. 5. Hence, based on standard results from robust control theory (Zhou et al., 1996; Sánchez Peña and Sznaier, 1998) derived from the small-gain theorem, the necessary and sufficient condition for stability, is:

$$\|W_\delta(s)T(s)\|_\infty < 1. \quad (9)$$

This represents the nominal closed-loop stability of the nonlinear saturation, for the case  $W_\delta = 1$ , and robust stability of the nonlinear uncertain model when  $W_\delta(s)$  has dynamics related to model uncertainty. This analysis assumes a small estimation error which in turn influences the value of the control signal  $u_{sat}$ . Based on the definitions in equations (6), the error  $\delta u = u_{sat} - \hat{u}_{sat}$  can be bounded as follows.

$$\delta u = f(\delta x) = \begin{bmatrix} f_E [W_{EE}\delta E(t) - W_{EI}\delta I(t)] \\ f_I [W_{IE}\delta E(t) - W_{II}\delta I(t)] \end{bmatrix}$$

where  $\delta E = E - \hat{E}$  and  $\delta I = I - \hat{I}$  are the estimation errors. The worst case scenario corresponds to the maximum slope of the sigmoid function  $f(x)$ , in this case  $x_{wc} = \theta$ , i.e.  $f(x_{wc}) = 0.5 - k$ . Therefore:

$$(\delta u)_{wc} = (0.5 - k) \begin{bmatrix} W_{EE} & -W_{EI} \\ W_{IE} & -W_{II} \end{bmatrix} \begin{bmatrix} \delta E \\ \delta I \end{bmatrix} \quad (10)$$

Therefore, a simplified implementation should verify that this value does not influence the control signal  $u_{sat}$ , i.e.  $\frac{\|(\delta u)_{wc}\|}{\|u_{sat}\|} < \xi_e$ , for a (small) predefined value  $\xi_e$ .

Additionally, a more elaborated solution would include an uncertainty block  $\hat{\Delta}$  which adds to  $u_{sat}$  in Fig. 5 and has as an input the Kalman filter error  $\delta x = \delta y = (y - \hat{y})$ . The robust stability condition, therefore, would be based on the structured singular value  $\mu_\Delta$  with structure  $\Delta = \text{diag}(\Delta, \hat{\Delta})$ , instead of the previous one, based on the  $\mathcal{H}_\infty$  norm in equation (9). However, without loss of generality, this is out of the scope of this work.

## 4. ILLUSTRATIVE EXAMPLE

### 4.1 Controller design

Physiological reasons guarantee that the values  $\tau_E, \tau_I$  are positive, hence, the LTI system  $G(s)$  is internally stable and additionally it has minimum phase. Moreover, since the coupling between sub-populations is lumped inside the sigmoid functions (input term  $u_{lti}$ ), the formulation introduced in (3) decouples the state variables  $E$ , and  $I$ . Therefore, the plant is amenable to synthesis approaches for open-loop stable systems, as well as independent design of SISO controllers  $K_I, K_E$  for each variable. To achieve the desired output (5), the controllers act on the  $P$  and  $Q$  inputs shifting the sub-population activity levels accordingly.

The structure of the proposed controller is based on the internal model control (IMC) (Morari, 1987) concept for stable models:

$$K_{LTI}(s) = q(s) [I - q(s)G(s)]^{-1}, \quad (11)$$

$$q(s) = F(s)G(s)^{-1}, \quad (12)$$

where  $F(s)$  is a low-pass filter, that guarantees stability and realizability of  $q(s)$ . In this case, the closed-loop I/O transfer matrix, i.e. the complementary sensitivity function, using equations (8),(11) and (12) is:

$$T(s) = q(s)G(s) = F(s).$$

The stabilizing LTI controllers, in this case,

$$K_{LTI}(s) \triangleq \begin{bmatrix} K_E(s) & 0 \\ 0 & K_I(s) \end{bmatrix} = \begin{bmatrix} \frac{5(s+1)}{s} & 0 \\ 0 & \frac{10(s+0.5)}{s} \end{bmatrix} \quad (13)$$

were designed as indicated previously and combined with the inverse sigmoid function and the state estimation to compute a nonlinear controller whose outputs  $(P, Q)$ , can be applied through optical means, as depicted in Fig. 3.

#### 4.2 Simulations

We propose a closed-loop pattern synchronization problem, in order to show the feasibility of the control framework. The patterns under consideration are brain rhythms, classified based on their frequency of oscillation. This example consists in a cross-frequency coupling (Hyafil et al., 2015), in the form of a top-down interaction between low frequency theta (frequencies between 4 Hz and 12 Hz) and high frequency gamma (up to 100 Hz approximately). The theta rhythm can modulate the gamma power of the intracortical LFP (Bragin et al., 1995; Lakatos et al., 2005), and is proposed to be a transient, long-range, coordination mechanism between different brain areas (Canolty et al., 2006), for communication in cognitive processing. For instance, the lack of this type of coupling can be linked with Alzheimer's disease (Zhang et al., 2016), thus the proposed strategy can be further developed as a potential treatment.

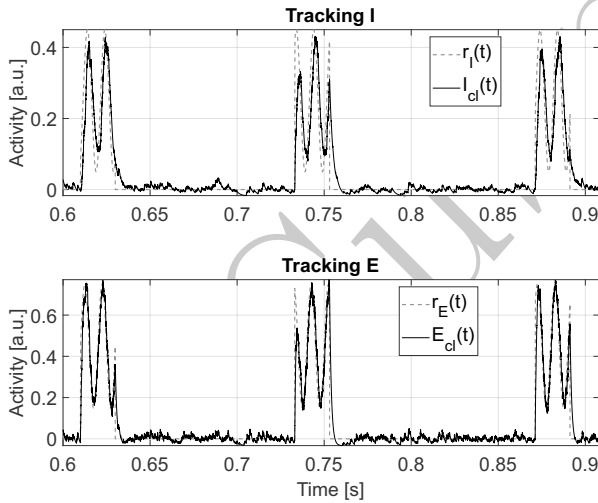


Fig. 6. The closed-loop tracking  $I_{cl}(t)$  and  $E_{cl}(t)$ , in bold lines, of the desired inhibitory  $r_I(t)$  and excitatory  $r_E(t)$  activities, in dashed lines. This is achieved with the applied control signals  $Q(t)$  and  $P(t)$ , as obtained with (7) and fed back to the system.

The local nature of the gamma rhythm (Srinivasan et al., 2013), allow us to choose a neural mass model of the Wilson-Cowan type. The interplay of the two interconnected sub-populations  $E, I$  in the form of fast excitation followed by delayed inhibition, showing limit-cycle behavior, may give rise to coherent oscillations in the gamma band (Buzsáki and Wang, 2012). Our objective is to induce oscillations in the high gamma range (i.e.  $f_t \approx 100$  Hz) using the model in a closed-loop manner, according to the amplitude variations of an ongoing theta rhythm occurring

simultaneously elsewhere. Specifically, we seek to use the troughs of the theta wave as a phase location window  $T_w(t)$ , as indicated with dashed lines in Fig. 7-a, and a pair of empirically-tuned sinusoidal references for local excitatory and inhibitory activities

$$r_E(t) = [0.3 \sin(2\pi f_t t) + 0.45] \cdot T_w(t), \quad (14)$$

$$r_I(t) = [0.2 \sin(2\pi f_t t - 0.94) + 0.25] \cdot T_w(t), \quad (15)$$

to achieve the closed-loop output  $y(t) = c_1 E_{cl}(t) + c_2 I_{cl}(t)$  shown in Fig. 7-b.

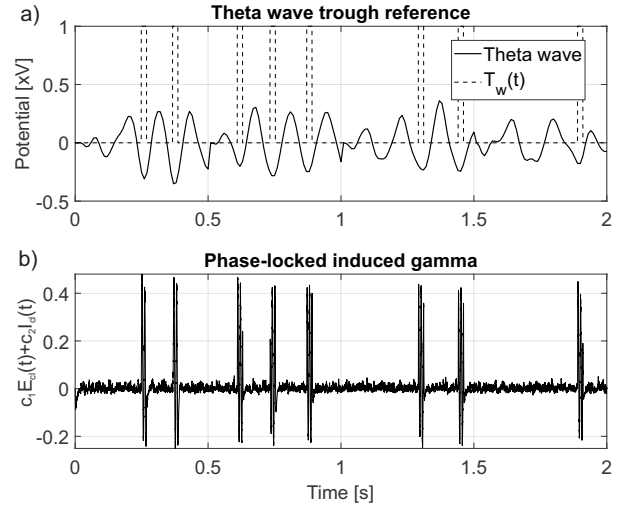


Fig. 7. a) The theta wave is acquired online (and band-passed between [4 12] Hz) for phase detection. The troughs found are used to conform a square wave  $T_w(t)$  that modulates the high gamma oscillation for reference. b) The output of the system is, consequently, phase-locked with the ongoing theta wave.

Since we want to track oscillatory levels of neural activity to induce certain rhythms, and these fluctuations are expected around a baseline level (DC component), the desired complementary sensitivity function will require good tracking in the frequency range  $[0, f_t]$ . That is, approximately unity gain from DC to the maximum tracking frequency  $f_t$  of interest.

The simple, phase-shifted references use parameters tuned to mimic the natural response of the system to stimulation (excitatory activity of greater amplitude and delayed inhibitory activity), but in this case, they are precisely tracked, as depicted in Fig. 6, with a closed-loop strategy. The open-loop response to an arbitrary stimulation pattern is shown in Fig. 8-c. The resulting trajectories, correspond to transient oscillations in the gamma range. The phase-locked, theta-gamma synchronization is shown in Fig. 8-b. The system alternates between a resting state of basal activity (the origin), and an oscillatory behavior, hence the limit cycle resemblance in the phase space. All trajectories have been processed with a low pass FIR filter with  $f_c = 300$  Hz, for visual clarity.

## 5. CONCLUDING REMARKS

We have presented a control framework for pattern tracking *in silico*, using a well-established system of excitatory

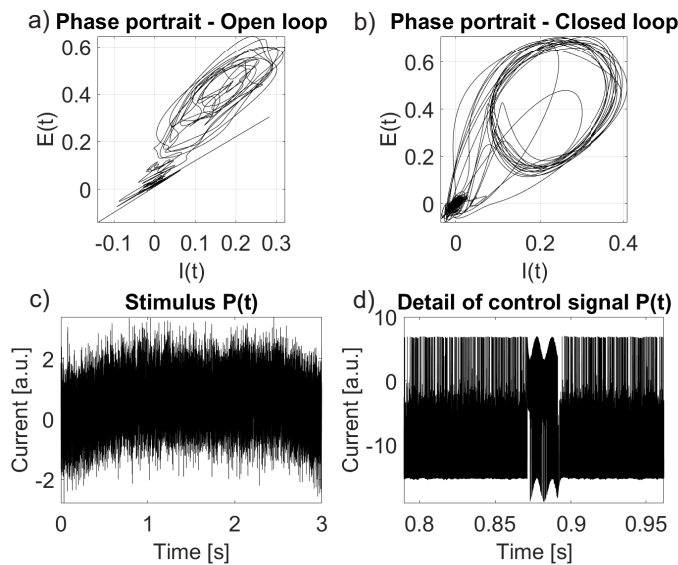


Fig. 8. System trajectories in the  $I$ - $E$  phase space. a) erratic quasi-oscillatory behavior in the gamma range, evoked by the trapezoidal, noisy excitatory-input, shown in c). The closed-loop control signal  $P(t)$  in d) is injected to the system (along with  $Q(t)$ , not shown) alternating between the baseline activity level, the origin, and the structurally stable oscillations of fixed frequency  $f_t$  as shown in b).

and inhibitory populations, as described by the Wilson-Cowan model. Although a particular IMC control strategy has been applied, to demonstrate the feasibility of the framework, other linear control strategies could be used as well. Note that a specific rhythm on the system, analogously to its natural oscillatory response to sufficient excitation, but on precise time windows, has been induced. This particular application could be further expanded to explore the functional phase-amplitude coupling.

For an experimental application, model (in)-validation is needed to obtain a nominal model and an uncertainty bound, to fulfill robustness and performance requirements. Also, as a future aspect to be explored, a more constrained control strategy using only one opsin can be potentially advantageous. This is due to technical complexities associated with opsins expression. Measuring only one activity, e.g. the excitatory population rate, can also reduce significantly the associated costs of the setup.

## REFERENCES

Bragin, A., Jandó, G., Nádasdy, Z., Hetke, J., Wise, K., and Buzsáki, G. (1995). Gamma (40-100 Hz) oscillation in the hippocampus of the behaving rat. *Journal of neuroscience*, 15(1), 47–60.

Buzsáki, G. and Wang, X.J. (2012). Mechanisms of gamma oscillations. *Annual review of neuroscience*, 35, 203–225.

Canolty, R.T., Edwards, E., Dalal, S.S., Soltani, M., Nagarajan, S.S., Kirsch, H.E., Berger, M.S., Barbaro, N.M., and Knight, R.T. (2006). High gamma power is phase-locked to theta oscillations in human neocortex. *Science*, 313(5793), 1626–1628.

Coombes, S. and Byrne, Á. (2019). Next generation neural mass models. In *Nonlinear dynamics in computational*

*neuroscience*, 1–16. Springer.

Deisseroth, K. (2011). Optogenetics. *Nature methods*, 8(1), 26–29.

Deubner, J., Coulon, P., and Diester, I. (2019). Optogenetic approaches to study the mammalian brain. *Current Opinion in Structural Biology*, 57, 157–163.

Faedo, N., García-Violini, D., and Ringwood, J.V. (2021). Controlling synchronization in a complex network of nonlinear oscillators via feedback linearisation and  $\mathcal{H}_\infty$ -control. *Chaos, Solitons & Fractals*, 144, 110722.

Hyafil, A., Giraud, A.L., Fontolan, L., and Gutkin, B. (2015). Neural cross-frequency coupling: connecting architectures, mechanisms, and functions. *Trends in neurosciences*, 38(11), 725–740.

Kim, E.H., Chin, G., Rong, G., Poskanzer, K.E., and Clark, H.A. (2018). Optical probes for neurobiological sensing and imaging. *Accounts of chemical research*, 51(5), 1023–1032.

Lakatos, P., Shah, A.S., Knuth, K.H., Ulbert, I., Karmos, G., and Schroeder, C.E. (2005). An oscillatory hierarchy controlling neuronal excitability and stimulus processing in the auditory cortex. *Journal of neurophysiology*, 94(3), 1904–1911.

Mirza, K.B., Golden, C.T., Nikolic, K., and Toumazou, C. (2019). Closed-loop implantable therapeutic neuromodulation systems based on neurochemical monitoring. *Frontiers in neuroscience*, 13, 808.

Morari, M. (1987). Robust process control. *Chemical engineering research & design*, 65(6), 462–479.

Powers, R.K. and Binder, M.D. (2001). Input-output functions of mammalian motoneurons. *Reviews of physiology, biochemistry and pharmacology*, 137–263.

Ribeiro, M.I. (2004). Kalman and extended kalman filters: Concept, derivation and properties. *Institute for Systems and Robotics*, 43, 46.

Sánchez Peña, R.S. and Sznajder, M. (1998). *Robust Systems Theory and Applications*. John Wiley & Sons.

Srinivasan, R., Thorpe, S., and Nunez, P.L. (2013). Top-down influences on local networks: basic theory with experimental implications. *Frontiers in computational neuroscience*, 7, 29.

Williams, J.C., Xu, J., Lu, Z., Klimas, A., Chen, X., Ambrosi, C.M., Cohen, I.S., and Entcheva, E. (2013). Computational optogenetics: empirically-derived voltage- and light-sensitive channelrhodopsin-2 model. *PLoS computational biology*, 9(9), e1003220.

Wilson, H.R. and Cowan, J.D. (1972). Excitatory and inhibitory interactions in localized populations of model neurons. *Biophysical journal*, 12(1), 1–24.

Wilson, H.R. and Cowan, J.D. (2021). Evolution of the Wilson-Cowan equations. *Biological cybernetics*, 115(6), 643–653.

Zhang, X., Zhong, W., Brankač, J., Weyer, S.W., Müller, U.C., Tort, A.B., and Draguhn, A. (2016). Impaired theta-gamma coupling in app-deficient mice. *Scientific reports*, 6(1), 1–10.

Zhou, K., Doyle, J.C., and Glover, K. (1996). *Robust and Optimal Control*. Prentice-Hall.